One-dimensional density waves of ultracold bosons in an optical lattice

C. Kollath
Institut für Theoretische Physik C, RWTH-Aachen, D-52056 Aachen, Germany and Sektion Physik, Ludwig-Maximilians-Universität, Theresienstrasse 37/III, D-80333 München, Germany

U. Schollwöck
Institut für Theoretische Physik C, RWTH-Aachen, D-52056 Aachen, Germany

J. von Delft
Sektion Physik, Ludwig-Maximilians-Universität, Theresienstrasse 37/III, D-80333 München, Germany

W. Zwerger
Institute for Theoretical Physics, Universität Innsbruck, Technikerstrasse 25, A-6020 Innsbruck, Austria
(Received 16 November 2004; published 13 May 2005)

We investigate the propagation of density-wave packets in a Bose-Hubbard model using the adaptive time-dependent density-matrix renormalization group method. We discuss the decay of the amplitude with time and the dependence of the velocity on density, interaction strength, and the height of the perturbation in a numerically exact way, covering arbitrary interactions and amplitudes of the perturbation. In addition, we investigate the effect of self-steepening due to the amplitude dependence of the velocity and discuss the possibilities for an experimental detection of the moving wave packet in time-of-flight pictures. By comparing the sound velocity to theoretical predictions, we determine the limits of a Gross-Pitaevskii- or Bogoliubov-type description and the regime where repulsive one-dimensional Bose gases exhibit fermionic behavior.

DOI: 10.1103/PhysRevA.71.053606 PACS number(s): 03.75.Kk, 05.30.Jp, 03.75.Lm

I. INTRODUCTION

The study of strong interactions in one-dimensional Bose gases has recently attracted considerable interest, in particular the suggestion of Petrov *et al.* [1] that in sufficiently dilute gases a regime appears in which one-dimensional (1D) bosons exhibit properties similar to those of a noninteracting Fermi gas. Following the realization of single-mode atomic wires by using strong 2D optical lattices [2], this so-called Tonks gas regime has indeed been seen in recent experiments [3,4].

Our aim in the present work is to study the propagation of density waves in strongly interacting one-dimensional Bose-Einstein condensates. Quite generally, the low-lying excitations in a Bose-Einstein condensate are soundlike and correspond to fluctuations of the condensate phase [5,6]. The associated sound velocity depends on both the density and interaction strength and is difficult to calculate microscopically in general. Beyond the weak-interaction limit, where a Gross-Pitaevskii or Bogoliubov description applies, very few results are available, except for the particular case of one dimension. In that case an exact solution for the ground state and the elementary excitations is available for the continuum model with a short-range interaction through the well-known Lieb-Liniger solution of the 1D Bose gas [7,8]. Experimentally, density perturbations can be created by applying a localized potential to the system with a far-detuned laser beam [9,10]. Alternatively, a phase imprinting method can be used, which allows one to create solitonic excitations [11,12].

In our present work, we study the evolution of density-wave packets in a one-dimensional system of ultracold bosons which are subject to an optical lattice along the axial direction. In previous studies, the motion of Gaussian wave packets has been investigated theoretically for small density perturbations or broad perturbations in three dimensions both with and without an optical lattice [14–16]. The sound velocity in an optical lattice was studied in [17]. These investigations were confined to the regime of weak interactions, describing properly systems with many particles per site. Here, we focus on the case of one-dimensional systems at low filling, i.e., with approximately one or less than one particle per site on average. This regime is of particular interest, since it allows one to study the behavior of sound waves near the transition from a superfluid to a Mott-insulating regime, as has been realized experimentally by Stöferle *et al.* [18]. The creation of a density perturbation with the width of a few lattice sites should be possible in these systems by the application of a localized laser beam [19].

As first pointed out by Jaksch *et al.*, ultracold bosons in an optical lattice provide a perfect realization of the Bose-Hubbard model [Eq. (1)] [32], which contains the interplay between their kinetic energy and their on-site repulsive interaction. The recently developed adaptive time-dependent density-matrix renormalization group method (adaptive t-DMRG) [21,22] is used to calculate the time evolution of wave packets. This method allows us to find the time evolution for both weak and strong coupling. In particular, it works best in an intermediate-interaction regime, where other methods are not reliable. We focus our investigation on the decay of the amplitude with time and on the sound velocity, i.e., the velocity of propagation of an infinitesimal perturbation. In addition, we determine the velocity of propagation of a perturbation with finite amplitude, thus entering

nonlinear effects which are difficult to discuss analytically even in one dimension.

We compare our numerical results in the limits of weak and strong interaction to different approximations. For weak interactions a continuum description is applied, which leads to a system of bosons with δ interaction, the Lieb-Liniger model [7,8]. We compare the resulting sound velocity with our results and find good agreement up to intermediate interaction strength. A further simplification is obtained by treating the Lieb-Liniger model in a hydrodynamical approach. The sound velocity determined by this approach is that of a Gross-Pitaevskii-type description. It agrees with our result only for rather small interaction strengths. In the limit of strong interactions and at low fillings, the Bose-Hubbard model can be mapped onto a model of spinless fermions [23]. As expected, our numerical results for the sound velocity in this limit smoothly approach the value predicted from this mapping to fermions [24].

The paper is organized as follows. We first introduce the Bose-Hubbard model, the analytical approximations, and the numerical method used. Then we investigate the motion of the wave packet. We analyze the decay of the amplitude of the perturbation and the dependence of the velocity, in particular the sound velocity, on system parameters like the background density, the interaction strength, and the height of the perturbation. Finally, we study how the presence of a wave packet can be detected experimentally from the interference pattern in a time-of-flight experiment.

II. MODEL

The Hamiltonian of the Bose-Hubbard model is given by

$$H = -J\sum_{j=1}^{L-1} b_j^\dagger b_{j+1} + \text{H . c .} + \frac{U}{2}\sum_{j=1}^{L} \hat{n}_j(\hat{n}_j - 1) + \sum_{j=1}^{L} \varepsilon_j \hat{n}_j, \tag{1}$$

where L is the number of sites in the chain, $b_j^\dagger$ and b_j are the creation and annihilation operators on site j, and $\hat{n}_j = b_j^\dagger b_j$ is the number operator [25]. In the limit of strong interactions, $u \gg 1$ with $u := U/J$, the atoms tend to localize. At integer filling $\tilde{\rho} = N/L = 1, 2\ldots$, where N is the total number of bosons, an incompressible Mott-insulating phase with locked density arises once u is increased beyond a critical value ($u_c \approx 3.37$ for $\tilde{\rho} = 1$ according to [26] in the thermodynamic limit). For weak interaction one finds a compressible superfluid phase. Experimentally [3,18,27], the parameter u can be varied over several orders of magnitude by changing the lattice depth. This allows one to tune through a superfluid–Mott-insulator transition, as first realized by Greiner *et al.* in a 3D optical lattice [27]. As mentioned before, it is possible to generate additional localized potentials using laser beams. These external potentials are modeled by the last term in Eq. (1). This term could as well describe arbitrary external potentials, e.g., a parabolic trapping [35] or more complicated structures. In the following we set $\hbar = 1$.

III. ANALYTICAL APPROXIMATIONS

For weak interactions, or quite generally for a description of the long-wavelength properties of a noncommensurate superfluid state, the continuum limit can be performed by taking $Ja^2 = \text{const}$ and $a \to 0$. In this limit the Bose-Hubbard model becomes equivalent to the Lieb-Liniger model [7,8],

$$H_{\text{LL}} = \int dx \left(\frac{1}{2M} |\partial_x \Psi(x)|^2 + V(x)\Psi^\dagger(x)\Psi(x) + \frac{g}{2}[\Psi^\dagger(x)]^2[\Psi(x)]^2 \right), \tag{2}$$

a bosonic model with δ interaction of strength g and external potential V. In this limit, the hopping parameter of the lattice model is related to the mass M of the atoms by $Ja^2 = 1/2M$ and the interaction strength to the δ-interaction strength by $Ua = g$.

Starting from this continuum model and considering the interaction in a mean-field approximation, the Gross-Pitaevskii equation can be derived [5]. Within this approximation, the motion of density waves is described by the two coupled equations [6]

$$\frac{\partial \rho}{\partial t} + \frac{\partial (v\rho)}{\partial x} = 0,$$

$$M\frac{\partial v}{\partial t} + \frac{\partial}{\partial x}\left(\frac{M}{2} v^2 + V \right) + \frac{\partial}{\partial x}\left(g\rho - \frac{1}{2M}\frac{\partial_x^2 \sqrt{\rho}}{\sqrt{\rho}} \right) = 0. \tag{3}$$

Here $\rho = |\Psi|^2$ is the density and $v = (1/2iM)(\Psi^* \boldsymbol{\nabla} \Psi - \Psi \boldsymbol{\nabla} \Psi^*)/\rho$ the velocity field. This equation gives a good description for systems in high dimensions or one-dimensional systems with many particles per site. Linearizing the equations, one recovers the results of the hydrodynamical approach [5].

We now turn to the opposite limit of strong interactions. For low densities $\tilde{\rho} \leqslant 1$ and strong interactions, the Bose-Hubbard Hamiltonian can be mapped to an effective model of spinless fermions with correlated hopping and attractive interactions [23]:

$$H_F = -J\sum_{j=1}^{L} \left(c_{j+1}^\dagger c_j - \frac{2J\hat{n}_j}{U} c_{j+1}^\dagger c_{j-1} + \text{H . c.} \right) - \frac{2J^2}{U}\sum_{j=1}^{L} (\hat{n}_{j+1} + \hat{n}_{j-1})\hat{n}_j + O(J^3/U^2), \tag{4}$$

where $\{c_j, c_{j'}^\dagger\} = \delta_{j,j'}$, anticommuting otherwise, and $\hat{n}_j = c_j^\dagger c_j$. Due to the correction $O(J^3/U^2)$, this mapping is only valid for $u \gg 1$.

IV. METHOD

To study the evolution of a free wave packet in a homogeneous system we apply the recently developed adaptive t-DMRG [20,21]. The adaptive t-DMRG is a numerical method based on the well-known static DMRG [28–30] and the time-evolving block-decimation (TEBD) procedure developed by Vidal [22]. The method describes the time evolution of wave functions in an essentially exact manner (for a detailed error analysis see [31]). In the calculation, the

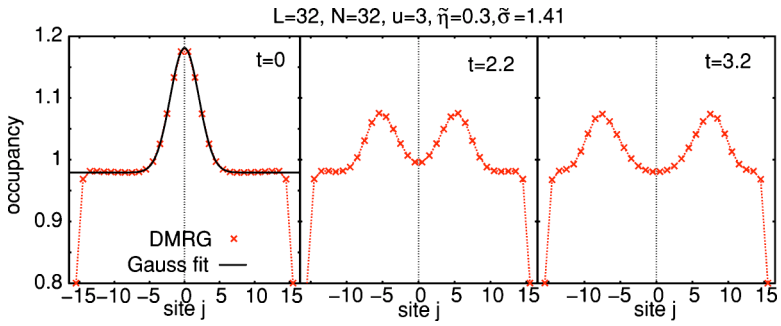

FIG. 1. Snapshots of the evolution of the density distribution are shown at different times. At $t=0$, a Gaussian wave packet is present in the center of the system. It splits up into two packets which move with the same speed in opposite directions.

infinite-dimensional bosonic Hilbert space on a single site is truncated to a finite value N_B. We checked the consistency of our results by varying N_B. For a chain of length $L=32$ and not too high density, the results for $N_B=6$ and 9 agreed well. In the following we use units in which the lattice spacing $a=1$ and the hopping $J=1$ (recall $\hbar=1$). This means that times are measured in units of $\hbar/J$ and velocities in units of $aJ/\hbar$.

V. PREPARATION OF THE DENSITY PERTURBATION

To prepare a density perturbation in our system we apply in Eq. (1), for $t\leqslant 0$, an external potential ε_j of Gaussian form,

$$\varepsilon_j(t) = -2\tilde{\eta}\tilde{\rho}e^{-j^2/2\tilde{\sigma}^2}\theta(-t), \tag{5}$$

which is switched off for times $t>0$. We determine the initial state as the ground state of the corresponding Hamiltonian at $t=0$ using a finite-system DMRG algorithm. Since DMRG produces site-dependent matrix product states [13], it can easily deal with the inhomogeneous density in our setup.

For weak perturbations, this potential creates an approximately Gaussian density packet

$$\rho_j(t\leqslant 0) = \rho_0(1+2\eta e^{-j^2/(2\sigma^2)}). \tag{6}$$

Note the difference between the parameters $\tilde{\sigma}$ and $\tilde{\eta}$, which are used to describe the applied potential, and the parameters σ and η, which determine the resulting density profile. For weak perturbations $\sigma=\tilde{\sigma}$, and η is related to $\tilde{\eta}$ via the compressibility $\partial\tilde{\rho}/\partial\mu\sim 1/U$. The background filling ρ_0 differs from the filling $\tilde{\rho}$ not only by the effect of the perturbation but also by boundary effects.

One constraint for the description of the time evolution of a wave packet by the Bose-Hubbard model is that the bosons should not be excited to higher-lying energy bands induced by the periodic potential of the optical lattice [32]. Hence it is valid as long as the additional energy by the perturbation is much smaller than the level spacing of the energy bands. The energy change induced by the perturbation consists of two contributions: the change in the interaction energy and the change in the kinetic energy. The first can be approximated by $\Delta E_{\text{int}}=2\rho\Delta\rho U$, with $\Delta\rho\sim\eta\sigma$ and $U\approx g\int d^3x|w(x)|^4$, where $w(x)$ is the associated Wannier function. The set of Wannier functions is often used in the context of periodic potentials, since these functions are maximally localized at the potential minima. Here $w(x)$ is the Wannier function localized around $x=0$. The kinetic energy is dominated by the fast oscillations induced by the periodic lattice potential as long as the change in the density by the perturbation varies more slowly. Hence an upper bound for the change in the kinetic energy is given by $\Delta E_{\text{kin}}\sim J\Delta\rho$. In total we demand that $\Delta E\sim U\Delta\rho(J/U+2\rho)\ll\nu$, where ν is the energy level spacing obtained on approximating the wells by parabolic potentials. For $\rho\sim 1$ and $J/U\lesssim 1$, this condition is obeyed provided that $\eta\sigma\ll a_\perp^2/a_\parallel a_s\sim 10$, where a_s is the scattering length. The lengths $a_\perp$ and $a_\parallel$ are the oscillator lengths perpendicular and parallel to the quasi-one-dimensional system. The oscillator lengths are the length scales of the approximately parabolic potentials around the lattice minima. Note that in this section we restored the dependence on J for better comparability to experimental parameters.

VI. EVOLUTION OF THE WAVE PACKET

A simple description of the evolution of a Gaussian wave packet for weak interactions can be obtained from a hydrodynamical approach. Linearizing Eqs. (3), one obtains a linear wave equation. An initially Gaussian wave packet of height η and background density $\overline{\rho}$ therefore shows a time evolution of the form:

$$\rho(x,t) = \overline{\rho}[1+\eta(e^{-(x-vt)^2/2\sigma^2}+e^{-(x+vt)^2/2\sigma^2})]. \tag{7}$$

Note that the background density $\overline{\rho}$ in the continuum is related to the background density ρ_0 in the lattice system by $\overline{\rho}=\rho_0/a$, where the lattice spacing a is restored. The wave packet at $t=0$ thus splits into two packets, which travel with the same speed in opposite directions. Indeed this is the behavior found in our simulations at weak coupling. Figure 1 shows snapshots of the evolution of a density-wave packet created at time $t=0$. When the wave packets reach the boundaries, they are reflected back and after some time they meet again in the center of the system. The evolution of the density for up to four reflections is shown in Fig. 2 by a density plot, i.e., the height of the density is encoded in a gray-scale scheme. The bright lines indicate the motion of the wave packet, which splits into two packets moving toward the boundaries. After some time the pattern becomes less pronounced and a substructure arises due to the reflection and scattering of the wave packets.

VII. HEIGHT OF THE AMPLITUDE

Damski [14] has shown that, neglecting the last term in the Gross-Pitaevskii equation (3), the so-called quantum

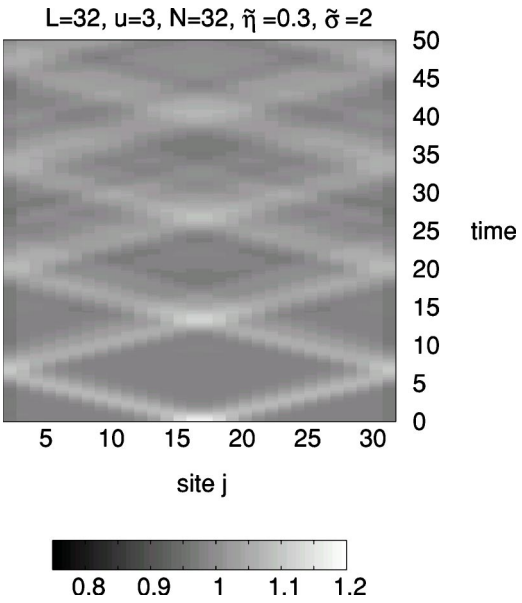

FIG. 2. Here the evolution of a density-wave packet is shown in a density plot. A linear gray scale is used, bright meaning higher densities. The bright lines correspond to the wave packets first splitting up, moving toward the boundaries, being reflected by the boundaries, and meeting again in the center of the system, where the cycle starts again. After some reflections a substructure arises due to boundary effects and packet interactions.

pressure term, the amplitude of the perturbation stays constant in time and equals $\overline{\rho}(1+\eta)$. A decay of the amplitude in this approximation occurs when the quantum pressure term become relevant. This term arises from the kinetic energy term and describes a restoring force due to spatial variations in the magnitude of the wave function of the condensate. It becomes important if the length scale of spatial variations is of the order of the healing length $\xi=1/(\sqrt{2\gamma\overline{\rho}})$, where γ is the dimensionless interaction strength defined by $\gamma=Mg/\overline{\rho}$. Hence a decay of narrow or high wave packets is expected even without an external potential. In agreement with this qualitative picture, our numerical results for the Bose-Hubbard model show that the decay becomes faster if (i) the width of the perturbation is narrower, and (ii) the amplitude of the perturbation is higher. As an example, in Fig. 3 the decay of the amplitude is shown for different amplitude heights and widths. Both plots show a very rapid decrease for small times [in (a) for $t<1$ and in (b) for $t<2$], which is due to the splitting of the wave packet. For larger times after the two wave packets are separated, the decay is approximately linear in time (this might be just the first contribution of a more complicated decay). Clearly, the decay of the amplitude of the initially small height $\tilde{\eta}\approx 0.1$ and width $\tilde{\sigma}\approx 1.4$ [Fig. 3(b)] is much slower than the decay of the amplitude of the initial height $\tilde{\eta}\approx 0.3$ and width $\tilde{\sigma}\approx 1$ [Fig. 3(a)]. The oscillations seen in the curve stem from the discrete structure of the lattice, since we plot the maximum value of the lattice occupancies over all lattice sites (and not the maximum of a fitted continuous curve which could lie between two lattice sites).

Due to the rather slow decay of small amplitudes, we determine in the following the values to be used for ρ_0, η,

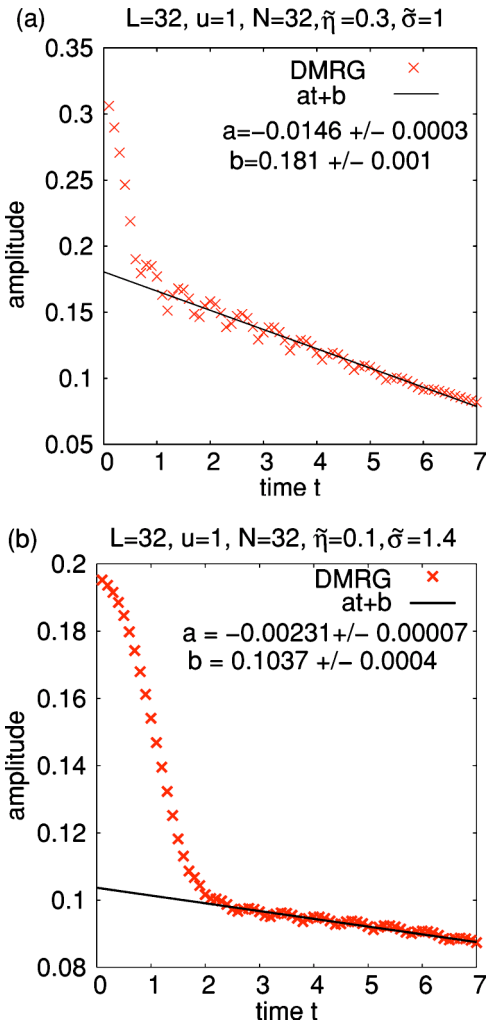

FIG. 3. The typical decay of the amplitude of the perturbation. We plot $(\rho_j)_{\max}-\rho_0$, i.e., the difference between the largest discrete site occupancy and the background occupation. The steep decrease for small times [up to $t\approx 1$ in (a) and $t\approx 2$ in (b)] corresponds to the splitting of the density-wave packet into two packets moving in opposite directions. The small oscillations in the curve stem from the discreteness of the underlying lattice. A linear fit is shown as a first approximation. For the lower and broader amplitude (b) a much slower decay is seen than for the amplitude (a).

and σ, by fitting the initial wave packet at $t=0$ to the form given by Eq. (6). Such a fit is shown in Fig. 1 at $t=0$. The error that results from assuming a time-independent amplitude η is negligible for small amplitudes and broad widths of the perturbation. The uncertainties of the numerical results for the density (determined by convergence checks in the number of DMRG states m, the allowed number of bosons N_B per site, and the Trotter time step Δt), and the errors made when reading off the parameters from the fit are much smaller than the size of the symbols used for data points in our plots (see for example Fig. 1).

VIII. SOUND VELOCITY

To investigate the dependence of the sound velocity on the background density ρ_0 and the interaction strength u in

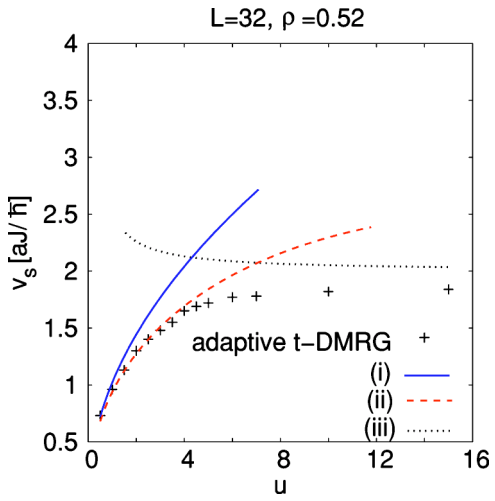

FIG. 4. The dependence of the sound velocity at constant background density $\rho_0=0.52$ on the interaction strength is shown. Our numerical results (+) are compared to (i) the results Eq. (9) of the hydrodynamical approach, (ii) the sound velocity determined by Lieb and Liniger Eq. (10), and (iii) the results Eq. (11) for strong interaction strength obtained by mapping onto spinless fermions. The results of Eq. (11), i.e., (iii), should become applicable for even stronger interactions than the ones shown here.

the Bose-Hubbard model, we create two small density perturbations with low amplitudes, a "bright" one, i.e., $\eta>0$, and a "gray" one, i.e., $\eta<0$ ($|\eta|<0.02$) at approximately the same background densities. Since the sound velocity is the velocity for an infinitesimal density perturbation and we simulate the motion of perturbations with finite amplitude, we interpolate between the two results for the velocity of the perturbations $\pm\eta$ linearly (this will be justified later on; see Sec. IX). The velocity is determined from the propagation of the maximum or the minimum of the density perturbation for $\pm\eta$, respectively. In Fig. 4 the sound velocity is plotted as a function of the interaction strength at fixed background density $\rho_0\approx 0.52$. (The background density can not be fixed easily to a certain value, since it depends on the total number of particles, the boundary effects and the perturbation. In our calculations it deviates from ρ_0 at most by 0.01.)

Our numerical results will be compared with the theoretical predictions from (i) a hydrodynamical approach or the linearized Gross-Pitaevskii equation, (ii) the Bogoliubov approximation for the continuum gas by Lieb, and (iii) the results of the mapping onto a spinless fermion model.

(i) The sound velocity determined by a hydrodynamical approach is given by

$$v(\bar{\rho},g)=\sqrt{g\bar{\rho}/M}. \tag{8}$$

Using the relations of the continuum limit, the corresponding velocity in the lattice is

$$v(\rho_0,u)=2\rho_0\sqrt{\gamma_{\mathrm{lat}}}, \tag{9}$$

with $\gamma_{\mathrm{lat}}=u/2\rho_0$ being the lattice analog of the dimensionless interaction.

(ii) As will be shown below, a much wider range of applicability than (i) is obtained from the results of Lieb for the continuous bosonic model [Eq. (2)] with δ interaction. They found two distinct modes of excitations, the usual Bogoliubov mode and the Lieb mode, which is associated with solitary waves [33]. At low momenta the dispersion relations for both modes have the same slope, which means that they propagate at the same sound velocity. The expression for the sound velocity can be obtained from the thermodynamic relation $Mv_s^2=\bar{\rho}\partial_{\bar{\rho}}\mu$, with μ as the chemical potential of the ground state, which is calculated within the Bogoliubov approximation. This results in [8]

$$v_s=v_{\mathrm{bare}}\frac{\sqrt{\gamma}}{\pi}\left(1-\frac{\sqrt{\gamma}}{2\pi}\right)^{1/2}, \tag{10}$$

where $v_{\mathrm{bare}}=\pi\bar{\rho}/M$ is the analog of the bare "Fermi" velocity. In order to relate that to the Bose-Hubbard model, we use the expressions obtained from the continuum limit, i.e., $\gamma\to\gamma_{\mathrm{lat}}$ and $v_{\mathrm{bare}}\to v_{\mathrm{bare,lat}}=2\pi\rho_0$. Within the continuum model, the numerical calculation of the sound velocity by Lieb shows that expression (10) is quantitatively correct up to $\gamma\sim 10$. By contrast the hydrodynamical result (9) is valid only up to $\gamma\approx 1$.

(iii) For strong interactions the sound velocity obtained by a mapping on a spinless fermion model is given by [24]

$$v_s^F\simeq v_F\left(1-\frac{8}{u}(\rho_0\cos\pi\rho_0)\right) \tag{11}$$

where the Fermi velocity of the lattice model is $v_F=2\sin\pi\rho_0$.

In Fig. 4 we compare these predictions to our numerical results. We see that for small interaction strength $u\lesssim 1$, i.e., $\gamma_{\mathrm{lat}}\lesssim 1$ (note that for $\rho_0=0.52$ and $u\approx\gamma_{\mathrm{lat}}$), the curves obtained using (i) and (ii) agree well with our numerical results. Around $\gamma_{\mathrm{lat}}\approx 1$ the mean-field prediction (i) starts to grow too fast, while the Bogoliubov approximation (ii) remains close to the numerical results up to intermediate interaction strength $\gamma_{\mathrm{lat}}\approx 4$. For even higher interaction strength also (ii) starts to differ significantly from our numerical results. This means that the lattice model starts to deviate from the continuum model, since (ii) was a very good approximation for the continuum model up to $\gamma\approx 10$. A breakdown of the continuum limit in this regime is expected, since the lattice analog of the healing length, i.e., $\xi_{\mathrm{lat}}=a/(\sqrt{2\gamma_{\mathrm{lat}}\rho_0})$, becomes of the order of the lattice spacing a and thus the discreteness of the lattice becomes relevant (we restored here the dependence on the lattice spacing a). The sound velocity in the lattice model always remains lower than in the continuum model. For higher interaction strength the numerical results approach the asymptotic value of prediction (iii). Note, that the prediction (iii) is only expected to become valid for even stronger interactions than shown here, since it is an expansion in u^{-1}. In Fig. 5 we see that our numerical results up to intermediate interaction strength show the dependence on the background density predicted by Eq. (10). Deviations from the predicted form occur for $\gamma_{\mathrm{lat}}\gtrsim 2$, depending on the particular set of parameters u and ρ_0. This dependence of the breakdown of the continuum limit (ξ_{lat} becomes of the order of a) is due to the fact that the healing length ξ_{lat} does not only depend on ρ_0 and u in the combination given by γ_{lat}.

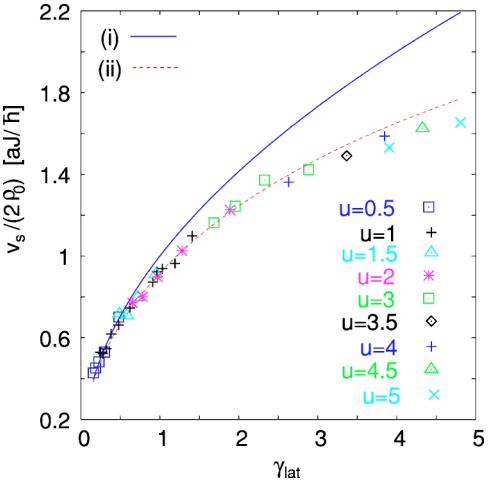

FIG. 5. The dependence of the sound velocity on the interaction strength and the background density is shown up to intermediate interaction strength. To confirm the prediction (ii) [Eq. (10)] we plot the ratio $v_s/(2\rho_0)$ versus $\gamma_{lat}=u/(2\rho_0)$.

Therefore deviations at smaller values of u arise for larger background densities. Alternatively, this may be expressed in the form shown in Fig. 5: the breakdown of the continuum limit occurs for larger u at smaller γ_{lat}.

To summarize, we find that the sound velocity as a function of the interaction strength shows a crossover between Eq. (10), where v_s/ρ_0 depends only on the combination of ρ_0 and u given by γ_{lat}, to a saturation at a value given by Eq. (11). In fact, a completely analogous behavior appears in the average kinetic energy of the particles, allowing one to identify the Tonks regime for quasi-1D tubes of bosons which are radially confined by a 2D optical lattice of increasing strength [4]. The breakdown of the prediction Eq. (10) is due to the discreteness of the lattice model and takes place if the healing length becomes of the order of the lattice spacing.

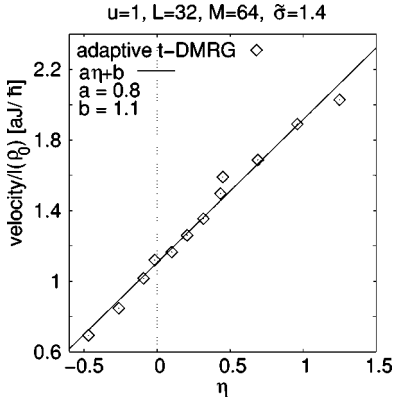

FIG. 6. The dependence of the velocity on the height of the amplitude η. The velocity is scaled by $l(\rho_0)$ to remove its dependence on the background density.

The results presented above were obtained using chain lengths between $L=32$ and 48 sites. Our numerical results for the time evolution of the density profile are converged in the number of states kept in the reduced space m (taken between $m=64$ and 96), which means that the Trotter error dominates the total error [31]. The errors in observables are very small (of the order of 0.0001) for Trotter time steps between $\Delta t=0.01$ and 0.05 and can safely be neglected in comparison to the uncertainties introduced by the determination of the sound velocity. For small interaction strength the velocity is relatively low and the movement over a long time can be fitted such that the accuracy of the results is of the order of ± 0.01 before interpolation between $\pm\eta$. For higher interaction strength, the uncertainty in the results for the velocity increases [approximately $O(\pm 0.05)$ for $u=6$]. This has two reasons. First, the velocity increases such that the end of the chain is reached in a rather short time. Moreover, oscillations in the density distribution induced by the finite size of

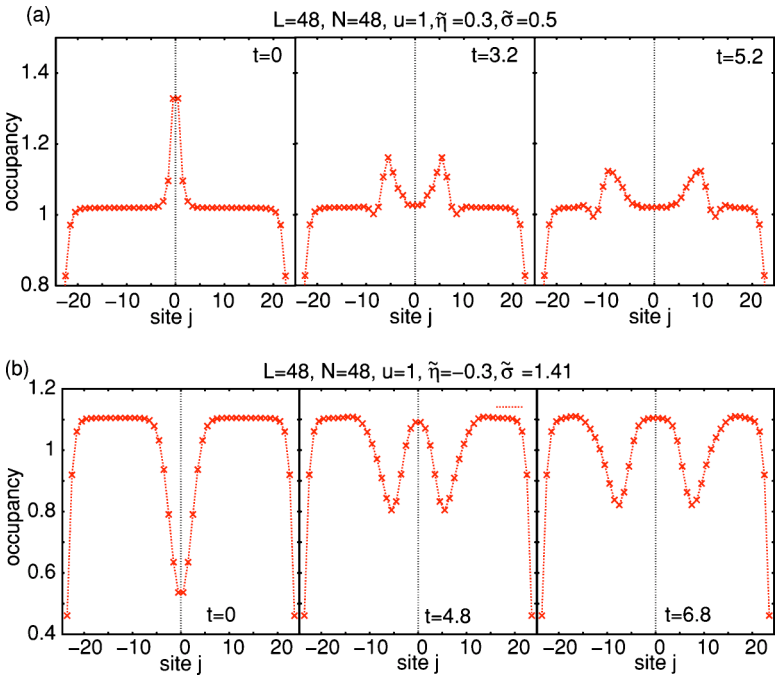

FIG. 7. The evolution of a narrow density-wave packet is shown for various fixed times. The wave packets undergo self-steepening and assume a symmetric form. The lines are guides to the eye.

the chain become more important and disturb the free evolution of the wave packets.

IX. SELF-STEEPENING

In Fig. 6 the dependence of the velocity on the height of the initial density-perturbation amplitude is shown. The data are taken at fixed interaction strength $u=1$ and different background densities ρ_0. The dependence of the velocity on the density is taken out by dividing by $l(\rho_0)\sqrt{2\rho_0}[1-(1/2\pi)(1/\sqrt{2\rho_0})]^{1/2}$ using our knowledge from the previous results [cf. Eq. (10), with $\gamma=\gamma_{\mathrm{lat}}=u/2\rho_0$, and $u=1$]. We see that for small amplitudes η, the dependence is approximately linear. It may be parametrized by $a\eta+b$ where $a=0.8$ and $b=1.1$. This linear dependence justifies the previously applied linear interpolation between $\pm\eta$ for the determination of the sound velocity.

As a consequence of the fact that the velocity increases monotonically with the amplitude of the perturbation, the wave can undergo self-steepening and shock-wave formation can occur [14,15]. One example where the phenomenon of self-steepening can be seen for a "bright" perturbation is shown in Fig. 7(a). The form of the density wave becomes very asymmetric. The front of the wave steepens and the back becomes more shallow. An additional dip arises at the front of the wave packet. This might stem from the discreteness of our system. In the case of a "gray" perturbation [Fig. 7(b)], the asymmetry develops the other way round; the front becomes more shallow and at the same time the back of the wave steepens. It should be emphasized, however, that the perturbations taken here are very narrow and high to have a strong effect. The Bose-Hubbard model might not be quantitatively applicable to describe such perturbations as discussed in Sec. V.

X. MOMENTUM DISTRIBUTION

Experimentally, one way of detecting the density perturbation is to take time-of-flight images [18,27]. Theoretically the interference pattern can be determined from the Fourier transform of the one-particle density matrix

$$I(k) = 1/N \sum_{j,j'=1}^{L} e^{i(j-j')ak}\langle b_j^\dagger b_{j'}\rangle,$$

neglecting its slowly varying envelope [34]. In a homogeneous system without a density perturbation a sharp interference peak appears at low interaction strength due to the long-range order in the one-particle density matrix. If the interaction increases beyond the point where a Mott-insulating phase is present, this peak broadens and decreases. Finally, for very strong interaction only a diffuse pattern is left [27,35]. In the presence of a density-wave packet, we find that a second interference peak appears at a finite momentum. In Fig. 8 we show the difference between an interference pattern at $t=0$, where the density wave is still in the center, and a later point, where the wave packets travel through the system. The possibility to resolve the second peak in the experiments depends on the parameters of the

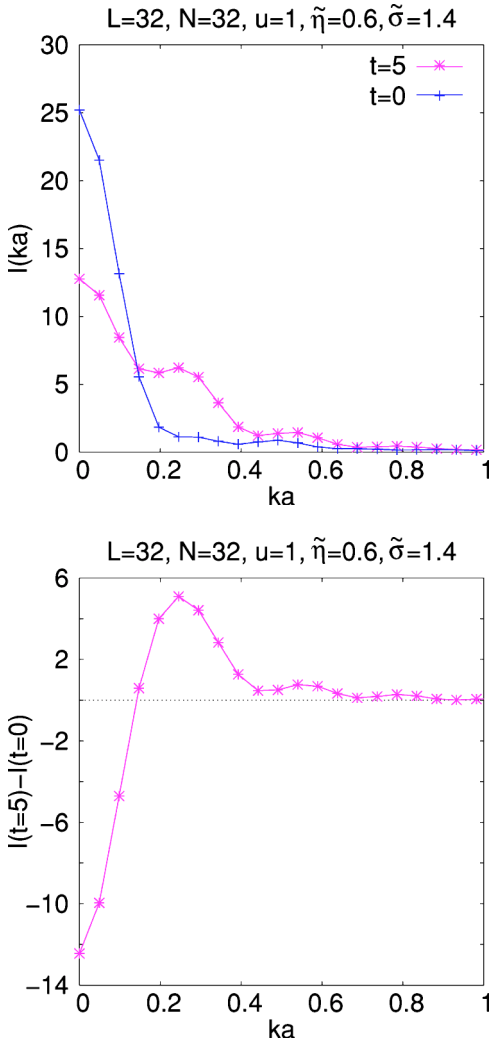

FIG. 8. On the left the interference pattern is shown for two different times. At $t=0$ only one sharp interference peak at $k=0$ exists. For times $t>0$ further peaks at finite momenta k and $-k$ arise, which correspond to the moving wave packets. Here only the region $k>0$ is shown, exploiting the symmetry under $k\rightarrow -k$. On the right the difference of the interference pattern for $t=5$ and 0 is shown. Here the errors are of the order of a few percent.

system. Specifically, the peak shown in Fig. 8 was calculated for a high amplitude of the density perturbation. This ensures that the mean number of bosons contributing to the second peak in the interference pattern is a sufficiently large fraction of the total boson number. In Fig. 8 the difference between the patterns at $t=5$ and 0 is shown.

In our investigations we neglected the transverse degrees of freedom. Small corrections to the sound velocity are expected by the coupling of the sound mode to these transverse degrees of freedom [36].

In the experimental realizations a parabolic trapping potential is present in addition to the periodic lattice. As a result, the background density is no longer homogeneous. Since the sound velocity depends on the background density, we expect it to vary for weak interactions according to Eq. (10) and for strong interactions according to Eq. (11). Only in the region where the trap varies slowly enough that the

background density is almost constant, we expect the trap to have negligible effect on the motion of the wave packet.

XI. SUMMARY AND OUTLOOK

To summarize, we investigated the motion of a wave packet in a Bose-Hubbard model which describes the dynamics of density perturbations in ultracold bosons in an optical lattice with a filling close to one particle per site. In the limit of weak interaction $\gamma \lesssim 1$, the motion of relatively broad and small perturbations can be described by the hydrodynamical approach or the linearized Gross-Pitaevskii equation. For intermediate interaction strength, however, the mean-field description breaks down while the results obtained from the corresponding continuum Lieb-Liniger model remain valid in this regime ($\gamma \lesssim 4$). For strong interactions, we found that the sound velocity is well approximated by a mapping onto a spinless fermionic model. In addition, we found a linear dependence of the velocity on the height of the amplitude. This gives rise to effects like self-steepening and shock-wave formation, in agreement with analytical predictions. Finally, we have shown that a density wave may be detected experimentally as an additional peak in the interference pattern.

Let us conclude by mentioning a few open questions. In the exact solution of the continuum model by Lieb and Liniger there are in fact two independent types of excitations. One of them exhibits a generalized Bogoliubov-type dispersion, which is linear at small momenta and crosses over to a quadratic free-particle behavior at large momenta. The other one only exists in a finite momentum range. It was later identified as the solitary wave of the nonlinear Schrödinger equation in 1D [33,37]. As was shown by Lieb and Liniger, the velocity of the dark solitons for repulsive interactions is always smaller than the linear sound velocity, coinciding with the latter only in the limit of long wavelengths. Experimentally, dark solitons have been observed in quasi-1D Bose-Einstein condensates, and have been identified by the fact that their velocity depends on the imposed phase gradient [11,12]. In the case of a deep lattice potential, as is studied here, solitary waves are predicted to appear in the weak-coupling regime $u \ll 1$ [38] and for sufficiently wide density perturbations which can be described by the 1D nonlinear Schrödinger equation. In addition, the presence of a lattice potential implies that atoms with momenta near a reciprocal lattice vector acquire a negative effective mass. This leads to the existence of bright gap solitons, a subject of considerable current interest [39–41], in particular in connection with instabilities for strongly driven optical lattices [42]. In this paper we focused our investigations mainly on the case of perturbations with small momenta, for which the two modes cannot be distinguished by their velocity. It is an open question to what extent the density waves in our simulations, can be interpreted as solitary waves and in particular what happens to these stable excitations in the regime of strong coupling, where the nonlinear Schrödinger equation no longer applies.

ACKNOWLEDGMENTS

We would like to thank M. Cazalilla, C. Tozzo, W. Hofstetter, T. Giamarchi, and E. Demler for fruitful discussions. C. K. was financially supported by Project No. DE 730/3-1 of the DFG and the Studienstiftung des deutschen Volkes. U. S. and W. Z. thank the Aspen Center for Physics, where parts of this work were carried out, for its hospitality and stimulating environment.

[1] D. Petrov, G. Shlyapnikov, and J. Walraven, Phys. Rev. Lett. **85**, 3745 (2000).
[2] H. Moritz, T. Stöferle, M. Köhl, and T. Esslinger, Phys. Rev. Lett. **91**, 250402 (2003).
[3] B. Paredes, A. Widera, V. Murg, O. Mandel, S. Fölling, I. Cirac, G. Shlyapnikov, T. Hänsch, and I. Bloch, Nature (London) **429**, 277 (2004).
[4] T. Kinoshita, T. Wenger, and D. Weiss, Science **305**, 1125 (2004).
[5] L. Pitaevskii and S. Stringari, *Bose-Einstein Condensation* (Oxford University Press, Oxford, 2003).
[6] C. J. Pethick and H. Smith, *Bose-Einstein Condensation in Dilute Gases* (Cambridge University Press, Cambridge, U.K., 2002).
[7] E. Lieb and W. Liniger, Phys. Rev. **130**, 1605 (1963).
[8] E. Lieb, Phys. Rev. **130**, 1616 (1963).
[9] M. Andrews, D. Kurn, H. Miesner, D. Durfee, C. Townsend, S. Inouye, and W. Ketterle, Phys. Rev. Lett. **79**, 553 (1997).
[10] M. R. Andrews, D. M. Stamper-Kurn, H.-J. Miesner, D. S. Durfee, C. G. Townsend, S. Inouye, and W. Ketterle, Phys. Rev. Lett. **80**, 2967 (1998).
[11] S. Burger, K. Bongs, S. Dettmer, W. Ertmer, K. Sengstock, A. Sanpera, G. Shlyapnikov, and M. Lewenstein, Phys. Rev. Lett. **83**, 5198 (1999).
[12] J. Denschlag *et al.*, Science **287**, 97 (2000).
[13] S. Östlund and S. Rommer, Phys. Rev. Lett. **75**, 3537 (1995).
[14] B. Damski, Phys. Rev. A **69**, 043610 (2004).
[15] C. Menotti, M. Krämer, A. Smerzi, L. Pitaevskii, and S. Stringari, Phys. Rev. A **70**, 023609 (2004).
[16] D. Boers, C. Weiss, and M. Holthaus, e-print cond-mat/0407617.
[17] A. Smerzi and A. Trombettoni, Phys. Rev. A **68**, 023613(2003).
[18] T. Stöferle, H. Moritz, C. Schori, M. Köhl, and T. Esslinger, Phys. Rev. Lett. **92**, 130403 (2004).
[19] I. Bloch (private communication).
[20] S. White and A. Feiguin, Phys. Rev. Lett. **93**, 076401 (2004).
[21] A. J. Daley, C. Kollath, U. Schollwöck, and G. Vidal, J. Stat. Mech.: Theory Exp. **2004**, P04005 (2004).
[22] G. Vidal, Phys. Rev. Lett. **93**, 040502 (2004).
[23] M. Cazalilla, Phys. Rev. A **67**, 053606 (2003).
[24] M. Cazalilla, e-print cond-mat/0406526.
[25] M. Fisher, P. Weichman, G. Grinstein, and D. Fisher, Phys. Rev. B **40**, 546 (1989).

[26] T. Kühner, S. White, and H. Monien, Phys. Rev. B **61**, 12474 (2000).
[27] M. Greiner, O. Mandel, T. Esslinger, T. Hänsch, and I. Bloch, Nature (London) **415**, 39 (2002).
[28] S. White, Phys. Rev. Lett. **69**, 2863 (1992).
[29] S. White, Phys. Rev. B **48**, 10345 (1993).
[30] U. Schollwöck, e-print cond-mat/0409292, Rev. Mod. Phys. (to be published).
[31] D. Gobert, C. Kollath, U. Schollwöck, and G. Schütz, Phys. Rev. E **71**, 036102 (2005).
[32] D. Jaksch, C. Bruder, J. Cirac, C. Gardiner, and P. Zoller, Phys. Rev. Lett. **81**, 3108 (1998).
[33] A. Jackson and G. Kavoulakis, Phys. Rev. Lett. **89**, 070403 (2002).
[34] V. Kashurnikov, N. Prokof'ev, and B. Svistunov, Phys. Rev. A **66**, 031601(R) (2002).
[35] C. Kollath, U. Schollwöck, J. von Delft, and W. Zwerger, Phys. Rev. A **69**, 031601(R) (2004).
[36] J.-P. Martikainen and H. T. C. Stoof, Phys. Rev. A **69**, 023608 (2004).
[37] M. Ishikawa and H. Takayama, J. Phys. Soc. Jpn. **49**, 1242 (1980).
[38] N. G. Parker, N. P. Proukakis, C. F. Barenghi, and C. S. Adams, J. Phys. B **37**, S175 (2004).
[39] O. Zobay, S. Pötting, P. Meystre, and E. Wright, Phys. Rev. A **59**, 643 (1999).
[40] I. Carusotto, D. Embriaco, and G. La Rocca, Phys. Rev. A **65**, 053611 (2002).
[41] W. Altman, A. Polkovnikov, E. Demler, B. Halperin, and M. Lukin, e-print cond-mat/0411047.
[42] L. Fallani, L. D. Sarlo, J. Lye, M. Modugno, R. Saers, C. Fort, and M. Inguscio, e-print cond-mat/0404045.